



INSTITUT DE FRANCE
Académie des sciences

Comptes Rendus

Géoscience

Sciences de la Planète


Mansour Rezaei Azizi, Ali Abedini and Samad Alipour

Application of lanthanides tetrad effect as a geochemical indicator to identify fluorite generations: A case study from the Laal-Kan fluorite deposit, NW Iran

Volume 352, issue 1 (2020), p. 43-58.

<<https://doi.org/10.5802/crgeos.2>>

© Académie des sciences, Paris and the authors, 2020.
Some rights reserved.

 This article is licensed under the
CREATIVE COMMONS ATTRIBUTION 4.0 INTERNATIONAL LICENSE.
<http://creativecommons.org/licenses/by/4.0/>



*Les Comptes Rendus. Géoscience — Sciences de la Planète sont membres du
Centre Mersenne pour l'édition scientifique ouverte*
www.centre-mersenne.org



Petrology, Geochemistry — Original Article

Application of lanthanides tetrad effect as a geochemical indicator to identify fluorite generations: A case study from the Laal-Kan fluorite deposit, NW Iran

Mansour Rezaei Azizi^{*},^a, Ali Abedini^a and Samad Alipour^a

^a Department of Geology, Faculty of Sciences, Urmia University, 5756151818, Urmia, Iran.

E-mails: manrezaei@yahoo.ca, m.rezaei@urmia.ac.ir (M. Rezaei Azizi), a.abedini@urmia.ac.ir (A. Abedini), alipour_samad@yahoo.com (S. Alipour).

Abstract. The Laal-Kan fluorite deposit situated in north margin of the Sanandaj-Sirjan metamorphic belt and Urmia-Dokhtar magmatic arc, NW Iran. The fluorite mineralization in the form of open-space filling, veins and veinlets have been deposited in the contact zone between highly metamorphosed schist, gneiss, amphibolite of the Paleozoic age and the Jangutaran limestone of the Precambrian age. The occurrence of convex tetrad effect and the calculated tetrad values indicate that early and late stage fluorite mineralization display various geochemical behavior, which are supported by the bivariate diagrams including T₁, T₃ and T₄ versus each other and some geochemical parameters such as La/Ho, Y/Ho and Zr/Hf ratios. It can, therefore, deduced that fluorite have been probably formed during two stages from hydrothermal fluids with a relatively constant composition. The fluid-rock interaction during deposition of fluorite and REE-F complex were likely the main mechanisms for the occurrence of tetrad effect.

Keywords. Lanthanides, Tetrad effect, Fluorite, Laal-Kan, Iran.

Manuscript received 26th April 2019, revised 3rd October 2019 and 13th October 2019, accepted 26th November 2019.

1. Introduction

Lanthanides and Y known as Rare Earth Elements (REE) generally occur in the trivalent oxidation state (Ln³⁺) except Ce (Ce³⁺ and Ce⁴⁺) and Eu (Eu²⁺ and Eu³⁺), which display very similar behavior during

geochemical processes in a wide range of geological environments [Bau and Dulski, 1995, Shannon, 1976]. This characteristic of REE have been used as a geochemical indicator for investigation of ore deposits and interpretation of the related geochemical processes during formation of deposits such as fluorite deposits [Abedini et al., 2019a, Ackerman, 2005, Akgul, 2015, Deng et al., 2014, Dill et al., 2016, Sasmaz and Yavuz, 2007, Sasmaz et al., 2018, Williams

^{*} Corresponding author.

et al., 2015]. The lanthanides are a coherent group of elements that their ionic radii gradually decrease with increasing the atomic number from La (1.03 Å) to Lu (0.86 Å), which is known as the lanthanide contraction [Shannon, 1976]. These specifications cause them to display similar behaviors and graphically smooth distribution patterns in geochemical investigations indicating their charge and radius controlling characteristic [Bau, 1996].

These irregularities have been interpreted as the existence and occurrence of the tetrad effect phenomenon in geochemical processes [Abedini *et al.*, 2018a,b,c, Kawabe, 1995, Lee *et al.*, 2013, Masuda *et al.*, 1987, Takahashi *et al.*, 2002], which have been reported for the first time by Fidelis and Siekierski [1966]. Lanthanides tetrads are known as four separate groups including La–Nd (first tetrad), Pm–Gd (second tetrad), Gd–Ho (third tetrad) and Er–Lu (fourth tetrad) correspond to 1/4, 1/2, 3/4 and filled electrons of $4f$ orbital in lanthanide elements [Jahn *et al.*, 2001]. As can be seen, Gd is a common element between second and third tetrads. The tetrad effect is another factor that controls the REE distribution beside other ones such as pH of fluids/solutions, scavenging, mineral phases and stability of REE-complex [McLennan, 1994, Sasmaz *et al.*, 2005, Veksler *et al.*, 2005].

Based on the recent works, the form of tetrad effect-bearing normalized REE curves can be categorized into four groups [Abedini and Rezaei Azizi, 2019, Abedini *et al.*, 2019b, Feng *et al.*, 2014, Minamim *et al.*, 1998, Nardi *et al.*, 2012]: (1) concave or W-type indicative for low temperature deposits, (2) convex or M-type generally occur in magmatic or related systems, (3) conjugate convex–concave or W–M-type and finally (4) zigzag pattern, which can be related to incomplete occurrence of tetrad effect. Previous studies have proposed some quantum mechanical based mechanisms for the occurrence of tetrad effect such as nephelauxetic ratios, the spin energy for coupling, electron configuration of lanthanides and Gibbs free energy [Jorgensen, 1970, Kawabe *et al.*, 1999, Masuda *et al.*, 1994, Nugent, 1970].

Fluorite deposits in Iran reach to 30 with being more than 3.4 million tones reserve. Some on these deposits are situated on the Sanandaj–Sirjan metamorphic belt including Qahr Abad, Bagher Abad, Darreh Badem, Atash Kuh and Laal-Kan [Alipour

et al., 2015, Ehya, 2012, Rezaei Azizi *et al.*, 2018b]. In this paper we focused on the behavior of the REE and some trace elements with emphasizes on the occurrence of tetrad effect in fluorite samples to constrain the difference between early and late stage fluorite precipitation in the hydrothermal fluorite deposit of the Laal-Kan district.

2. Geological settings

Previous studies indicated that many Zn–Pb and fluorite–barite deposits have been formed at the margins of the Central Iranian Zone [Rajabi *et al.*, 2012]. Based on the structural geology map of Iran [Aghanabati, 1998, Alavi, 1991], the Laal-Kan fluorite deposit is situated ~90 km west of Zanjan city, NW Iran at the contact zone of the Sanandaj–Sirjan metamorphic belt and Urmia–Dokhtar magmatic arc [Gilg *et al.*, 2006, Richards *et al.*, 2006] and a worldwide known Zn–Pb Angouran mine is located ~500 m south of the fluorite deposit (Figure 1).

The simplified geology map of the study district (Figure 2) shows that diverse lithologies from the Precambrian to Quaternary ages crop out in this district [Babakhani and Ghalamghash, 1990]. These lithologies from oldest to youngest can be summarized as follows: (1) the Kahar Formation including micaschist, gneiss, amphibolite and quartzite of the Neoproterozoic age, (2) a metamorphosed ultramafic–mafic lava and dolomitic limestone–limestone (Jangutaran Limestone) of the Precambrian age, (3) a highly metamorphosed alternation of schist, gneiss, marble and amphibolite of the Paleozoic age, (4) quartzdiorite, diorite, gabbro and granite of the Triassic–Jurassic age, (5) the Lower Red Formation including sandstone, conglomerate and gypsiferous marls of the Oligocene–Miocene age, (6) alternation of marl, sandstone, siltstone and mudstone of the Oligocene–Miocene age, (7) andesitic volcanic breccia of the Oligocene–Miocene age, (8) dacitic–ignibritic lavas and porphyritic andesitic lavas of the Oligocene–Miocene age, (9) limestone of Qom Formation of the Oligocene–Miocene age, (10) andesitic, dacitic–andesitic lava domes of the Oligocene–Miocene age, (11) travertine, sand, clay and recent alluvium of the Quaternary age.

Field observations reveal that fluorite mineralization in the form of open-space fillings, veins and veinlets are in the contact zone between the highly

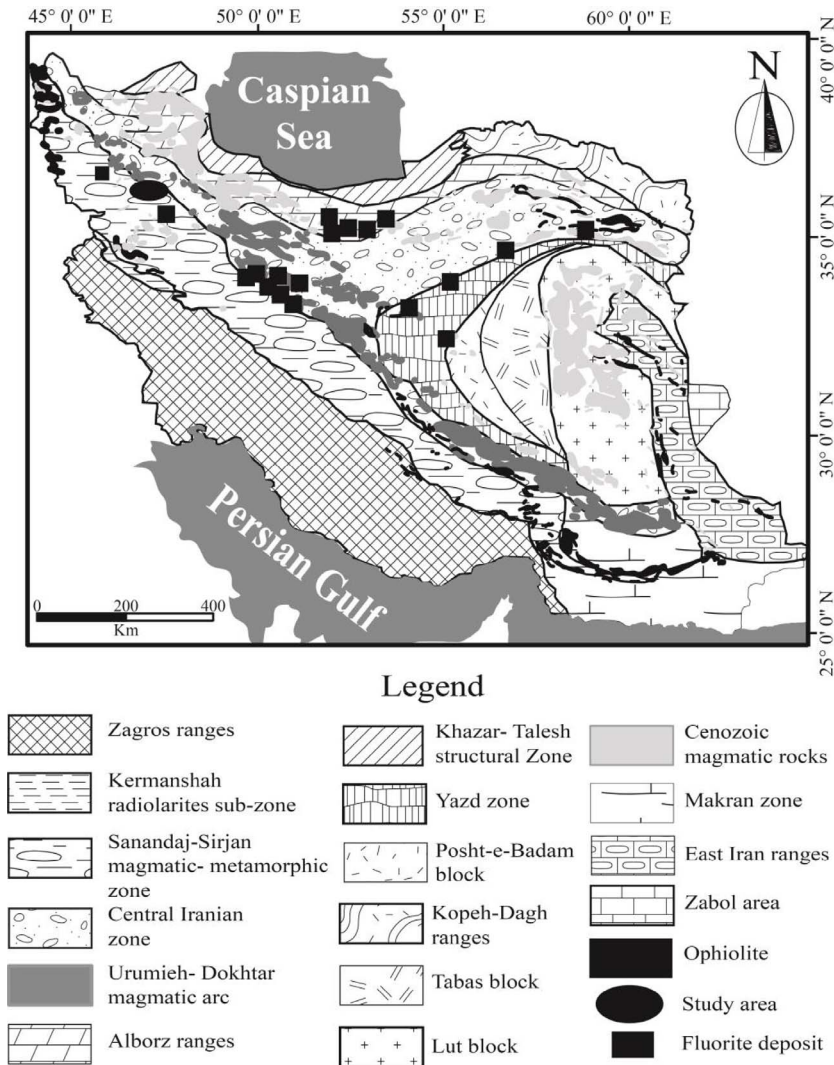


Figure 1. Simplified structural map of Iran [Alavi, 1991, Aghanabati, 1998] indicating the location of Laal-Kan and some fluorite deposits.

metamorphosed schist, gneiss, amphibolite of Paleozoic age and the Jangutaran limestone of the Precambrian age [Rezaei Azizi *et al.*, 2018b]), which deposited along and/or parallel to the Laal-Kan Fault in a W-E trending (Figure 2). The existence of a close relationship between the fault system and mineralization emphasizes that the structural systems have played a significant role as pathways for uprising hydrothermal fluids [Rezaei Azizi *et al.*, 2018b]. Fluorite mineralization in this deposit has a variable thickness from a few centimeters to ~4 m. Field observations indicate that the contact between mineraliza-

tion and host rocks are relatively sharp with no significant alteration. White, smoky and violet colors are the most abundant that can be seen in the study district.

3. Sampling and analytical methods

Thirty-seven samples of fluorite in white, smoky and violet colors from the excavated places of the deposit were collected for petrographic studies. In order to prevent any probable alteration and/or wall-rock interaction during our studies, fifteen thin sections of

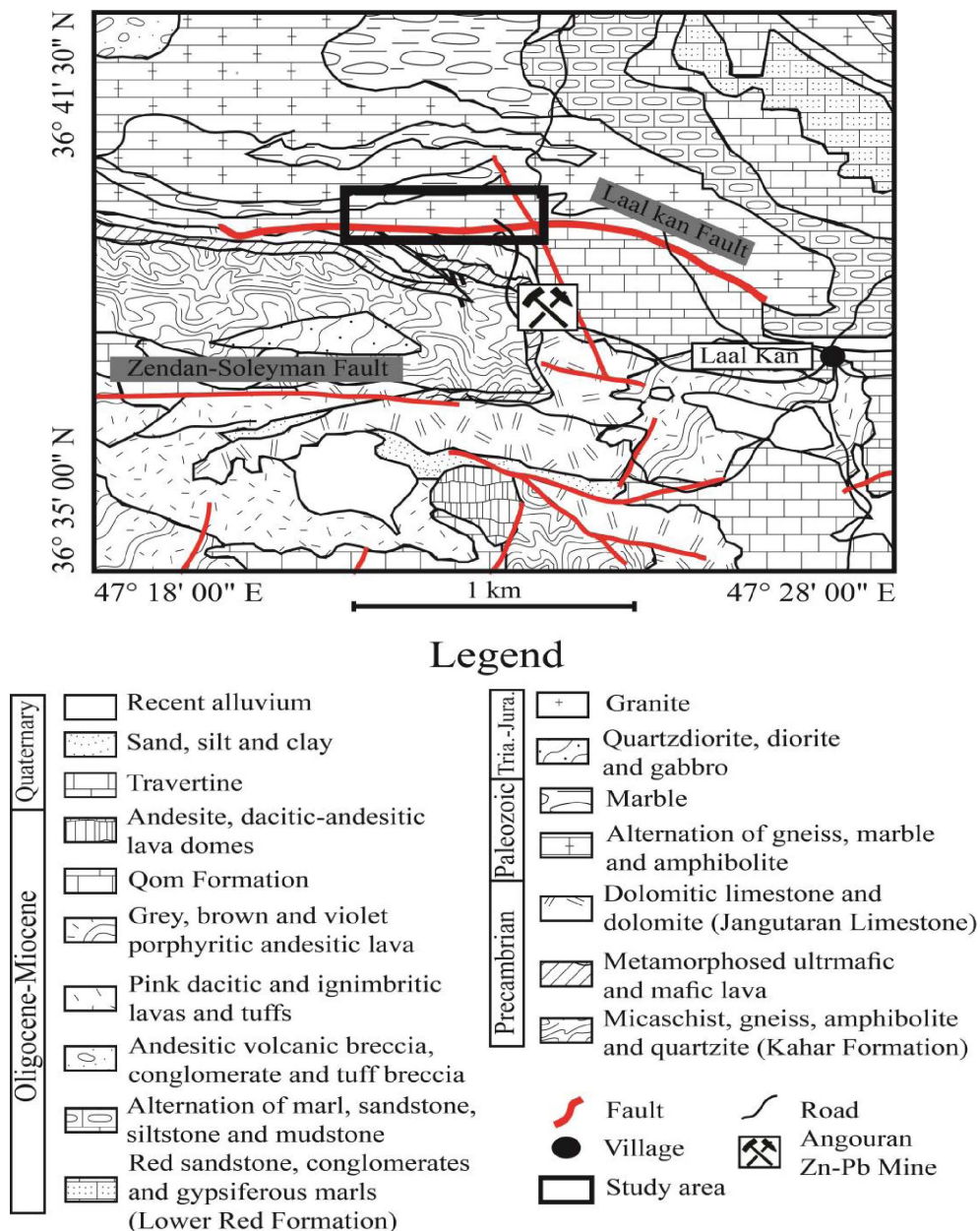


Figure 2. Simplified geology map of the study district (after Babakhani and Ghalamghash [1990]).

fluorite samples (in all available colors) were prepared and studied using a petrographic microscope in the Geology Department at Urmia University to determine the available mineral phases and their genetic relationship.

For chemical analysis, to prevent any contamination all fluorite grains were separated from the

host rocks by handpicking under a binocular microscope in the Geology Department at Urmia University. Totally, eleven fluorite samples (>99% purity) of the study district in various colors including white (#2), smoky (#2) and violet (#7) were analyzed using the inductively coupled plasma mass spectrometry (ICP-MS) technique to determine the

trace and REE concentration at the Zarazma Zangan Iranian Co, Iran.

For chemical analysis, all the prepared samples were crushed to less than –80 mesh after drying at a temperature less than 60 °C. 250 g of fluorite samples were powdered to less than –150 mesh using a steel ring mill and 0.2 g of these prepared fluorite samples were weighted. 1.5 g lithium borate ($\text{Li}_2\text{B}_4\text{O}_7$) was added to each of the fluorite samples and heated at 980 °C for ~30 min. After cooling these samples, each one of them was dissolved in 100 ml nitric acid (5%). For measuring the amount of trace and REE in each samples, they poured into a Polypropylene Test Tube. Measuring the loss on ignition (LOI) was calculated by the amount of weight loss of 1 g sample before and after heating at 950 °C for ~90 min. The calibration and standards were also carried out to control during analysis processes. The detection limits for analyzed elements including trace and REE varied from 0.02 to 5 ppm.

4. Results

4.1. Petrography

The mineralogy studies in the fluorite samples of this district showed that fluorite, quartz and Fe-oxides mostly hematite were the major mineral phases of the samples but, barite, calcite, hemimorphite and clays were distinguished as the minor mineral phases.

Based on the field observations, fluorite mineralization in the form of open-space fillings, veins and veinlets consisting of relatively coarse-grained and massive crystals, which display relatively sharp contact with schist (host rock). Hemimorphite and Fe-oxides are relatively abundant minor mineral phases that can be distinguished in the supergene zone due to weathering.

The studies indicate that fluorite mineralization has been probably formed in two different stages. Early stage fluorite crystals are characterized by large coarse-grained and massive euhedral to subhedral crystals (Figure 3a, b). These studies also indicated that tectonic activities caused micro fractures to be formed in the early stage fluorite crystals. These fractures were filled with Fe-oxides and clay mineral phases during weathering processes (Figure 3c, d). The early stage fluorite crystals were also associated

with first generation euhedral to subhedral quartz (Figure 3e, f). The late stage fluorite is characterized by subhedral to anhedral, fine-grained fluorite crystals, which were formed in the fractures of the early stage fluorite crystals and/or schist (host rock) at distance some far from the open-space filling and cavities in the study district (Figure 4a, b). The late stage fluorite in this district is associated with subhedral to anhedral fine-grained quartz (Figure 4c, d) and hemimorphite (Figure 4e, f).

4.2. Geochemistry

The concentrations of some trace and REE for fluorite samples in the Laal-Kan fluorite deposit are presented in Table 1. As shown in this table, the concentration of Y, Hf and Zr vary between 6.1–8.3, 0.65–1.61 and 0.8–4.7 ppm, respectively. The total REE values of the analyzed samples also vary in the range of 4.16–25.67 ppm. Table 2 also lists the calculated geochemical ratios for fluorite samples in the study district. The Zr/Hf ratio is in the range of 0.5–4.75. The Y/Ho and La/Ho ratio values for fluorite samples vary from 24.4 to 52.31 and from 2.88 to 24.92, respectively.

5. Discussion

5.1. REE geochemistry

REE distribution during geochemical processes is strongly dependent on some paleo physico-chemical conditions such as pH, Eh, temperature of fluids/solutions, fugacity of oxygen in the environment, water/rock interaction and REE-complex stability [Abedini *et al.*, 2011, Bau *et al.*, 2003, Castorina *et al.*, 2008, Khosravi *et al.*, 2017, Levresse *et al.*, 2011, Nkoumbou *et al.*, 2017, Rezaei Azizi *et al.*, 2018a, Sasmaz *et al.*, 2005, Tassongwa *et al.*, 2017]. Fluorite as an informative mineral has been reported from a wide range of deposits and geological environments that can be used to constraint the paleo physico-chemical condition during geochemical investigations [Coşanay *et al.*, 2017, Schwinn and Markl, 2005].

Statistically, the median values of REE concentration in fluorite samples of the study district is 8.41 ppm with the standard deviation equal to 8.5 ppm. The large value for calculated values of the standard deviation means that the distribution

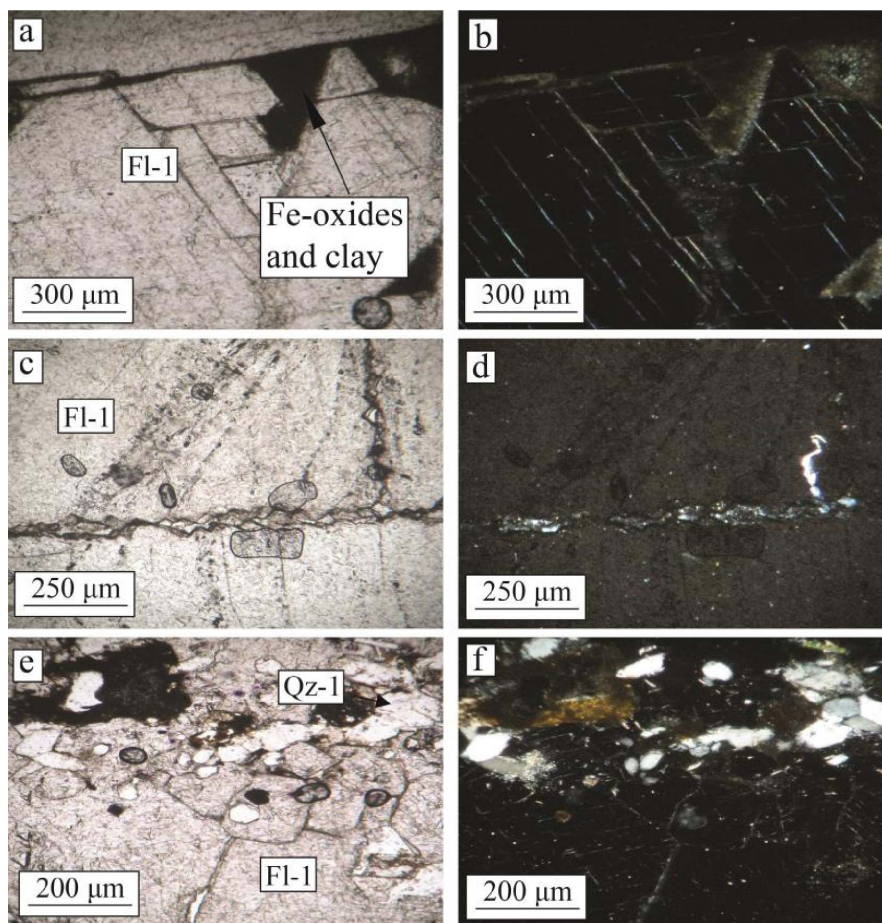


Figure 3. Photomicrographs of the early stage fluorite mineralization in the Laal-Kan deposit. (a) and (b) coarse-grained and massive early stage fluorite (Fl-1) filled with Fe-oxides and clay minerals under ppl and xpl lights, respectively. (c) and (d) the occurrence of micro fractures in the early stage fluorites (Fl-1) filled with quartz and calcite under ppl and xpl lights, respectively. (e) and (f) first generation euhedral to subhedral quartz (Qz-1) crystals in the early stage fluorite Fl-1 under ppl and xpl lights, respectively. Fl = fluorite and Qz = quartz. Abbreviations are from Whitney and Evans [2010].

pattern for Σ REE in fluorite samples is not a normal distribution [Edjabou *et al.*, 2017]. As shown in Figure 5a, the distribution patterns show two different peaks that can be related to different populations due to changes in geochemical condition during formation of fluorite [Abedini and Rezaei Azizi, 2019, Badel *et al.*, 2011]. The clusters were classified into two populations due to geological, geochemical and mathematical based relationships (Figure 5b, c). The first population includes the fluorite samples that are characterized by low Σ REE with the median and standard deviation values equal to 6.1 and 1.5 ppm,

respectively. The second group of samples has larger values of the median and standard deviation values equal to 21.6 and 2.9 ppm, respectively.

5.2. Tetrad effect

The chondrite-normalized REE patterns for fluorite samples are shown in Figure 6. Previous studies have shown that the early stage fluorite mineralization (Figure 6a) is characterized by LREE enrichment relative to HREE, whereas the late stage ones (Figure 6b) are characterized by LREE depletion [Rezaei Azizi

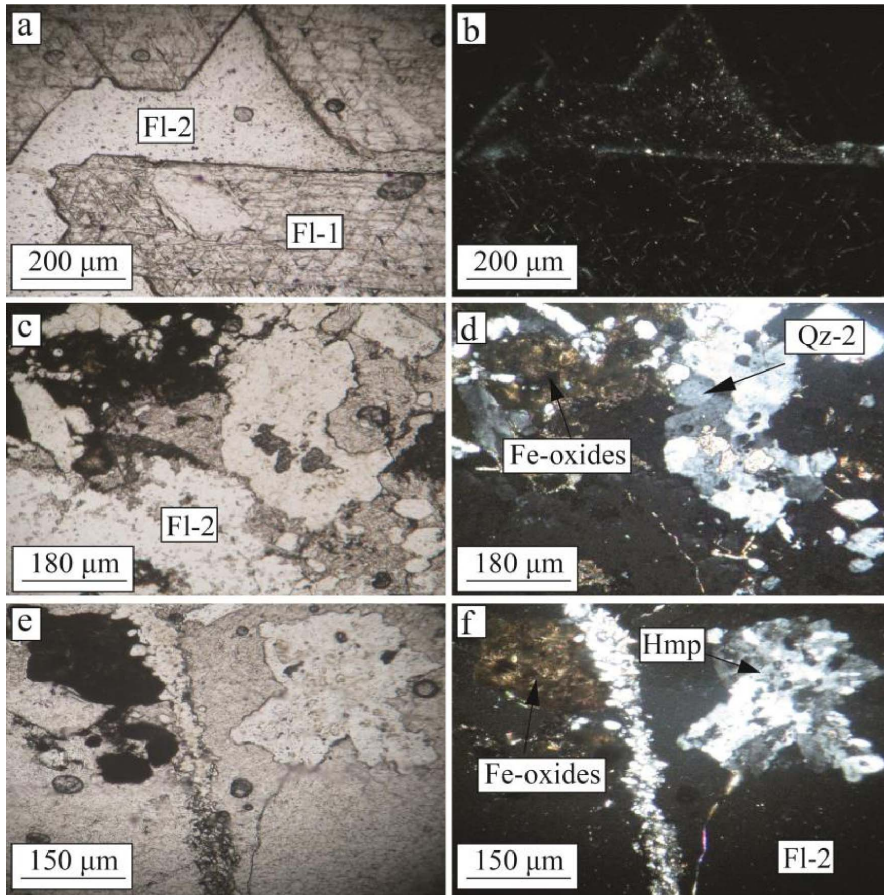


Figure 4. Photomicrographs of the late stage fluorite mineralization in the Laal-Kan deposit. (a) and (b) coarse-grained and massive early stage fluorite (Fl-1) and late stage fluorite (Fl-2) under ppl and xpl lights, respectively. (c) and (d) Fe-oxides and subhedral to anhedral fine-grained quartz associated with the late stage fluorites (Fl-2) under ppl and xpl lights, respectively. (e) and (f) hemimorphite in association with the late stage fluorite (Fl-2) under ppl and xpl lights, respectively. Fl = fluorite, Hmp = hemimorphite and Qz = quartz. Abbreviations are from Whitney and Evans [2010].

et al., 2018b). The remarkable point in these patterns is the occurrence of the tetrad effect in the fluorite samples of the Laal-Kan deposit. Both early and late stage fluorite samples display a convex form in the chondrite-normalized REE patterns. In this paper, the values of tetrad effect in each group were calculated by (1) proposed by Monecke *et al.* [2002].

$$T_i = \sqrt{\frac{1}{2} \times \left(\left[\frac{X_{Bi}}{\sqrt[3]{X_{Ai}^2 \times X_{Di}}} - 1 \right]^2 + \left[\frac{X_{Ci}}{\sqrt[3]{X_{Di}^2 \times X_{Ai}}} - 1 \right]^2 \right)} \quad (1)$$

In this equation, X_{Bi} and X_{Ci} are the concentrations of the two central elements of the individual tetrad, and X_{Ai} and X_{Di} the concentrations of the first and the fourth lanthanides of the same tetrad, respectively and T_i ($i = 1-4$) gives the values for each tetrad. If all tetrad elements are in the straight line T_i will be equal to zero and T_i values higher than zero indicate the occurrence of tetrad effect in the normalized curves. It is worth noting that radioactive Pm does not occur in geological environments, therefore the calculation of second tetrad is impossible [McLennan, 1994]. Table 3 lists the calculated values for individual tetrad in fluorite samples of the study deposit.

Table 1. The concentration values (in ppm) of some trace and REE for fluorite samples in the Laal-Kan fluorite deposit

Element	White fluorite		Smoky fluorite		Violet fluorite						
	WF.1	WF.2	SF.1	SF.2	VF.1	VF.2	VF.3	VF.4	VF.5	VF.6	VF.7
	Fl-1	Fl-2	Fl-1	Fl-1	Fl-1	Fl-2	Fl-2	Fl-2	Fl-2	Fl-2	Fl-1
Y	6.7	8.3	6.5	7.2	6.4	6.6	6.7	7.2	6.8	6.8	6.1
Hf	0.81	0.65	0.78	0.97	1.34	1.58	1.61	1.48	1.39	1.17	0.83
Zr	3.8	1.5	3.5	4.1	4.7	1.8	0.8	2.1	0.9	1.6	3.6
La	4.72	1.2	5.98	5.1	4.04	0.82	0.49	0.7	0.4	0.48	3.45
Ce	7.89	3.08	10.06	9.11	7.07	2.04	2.08	2.39	1.3	1.15	6.51
Pr	0.93	0.31	1.09	1.02	0.86	0.2	0.18	0.21	0.13	0.11	0.9
Nd	3.58	0.95	3.98	3.65	3.25	0.63	0.57	0.69	0.4	0.36	2.98
Sm	0.87	0.19	0.82	0.75	0.64	0.18	0.21	0.19	0.16	0.14	0.59
Eu	0.23	0.05	0.26	0.23	0.22	0.04	0.03	0.04	0.04	0.04	0.19
Gd	0.53	0.25	0.49	0.52	0.49	0.2	0.23	0.22	0.18	0.2	0.49
Tb	0.08	0.06	0.06	0.05	0.07	0.05	0.06	0.05	0.04	0.04	0.05
Dy	0.72	0.6	0.64	0.74	0.74	0.63	0.62	0.53	0.43	0.51	0.66
Ho	0.26	0.2	0.24	0.23	0.22	0.19	0.17	0.15	0.13	0.14	0.25
Er	0.84	0.65	0.98	0.81	0.92	0.64	0.6	0.53	0.43	0.5	0.89
Tm	0.12	0.12	0.14	0.13	0.14	0.11	0.1	0.09	0.07	0.08	0.15
Yb	0.75	0.69	0.84	0.85	0.76	0.58	0.51	0.47	0.4	0.46	1.02
Lu	0.08	0.06	0.09	0.08	0.08	0.05	0.05	0.04	0.05	0.04	0.1
ΣREE	21.6	8.41	25.67	23.27	19.5	6.36	5.9	6.3	4.16	4.25	18.23

Fl-1 = early stage fluorite and Fl-2 = late stage fluorite.

Table 2. The calculated geochemical ratios (mass ratios) for fluorite samples in the Laal-Kan fluorite deposit

Ratios	White fluorite		Smoky fluorite		Violet fluorite						
	WF.1	WF.2	SF.1	SF.2	VF.1	VF.2	VF.3	VF.4	VF.5	VF.6	VF.7
Zr/Hf	4.75	2.31	4.49	4.23	3.51	1.14	0.50	1.42	0.65	1.37	4.34
Y/Ho	25.77	27.08	36.09	29.09	24.40	28.00	34.74	39.41	48.00	52.31	48.57
La/Ho	18.15	24.92	22.17	18.36	13.80	6.00	4.32	2.88	4.67	3.08	3.43

According to these results, the early stage fluorite samples are characterized by low T_1 , high T_3 and low T_4 values, whereas in the late stage fluorite samples T_1 , T_3 and T_4 values are high, low and high, respectively. Figures 7 illustrate the bivariate diagrams of tetrad effect values in the fluorite samples. As shown in these figures, first tetrad has negative correlation versus third tetrad values (Figure 7a). These trends can be seen in both first versus fourth and third

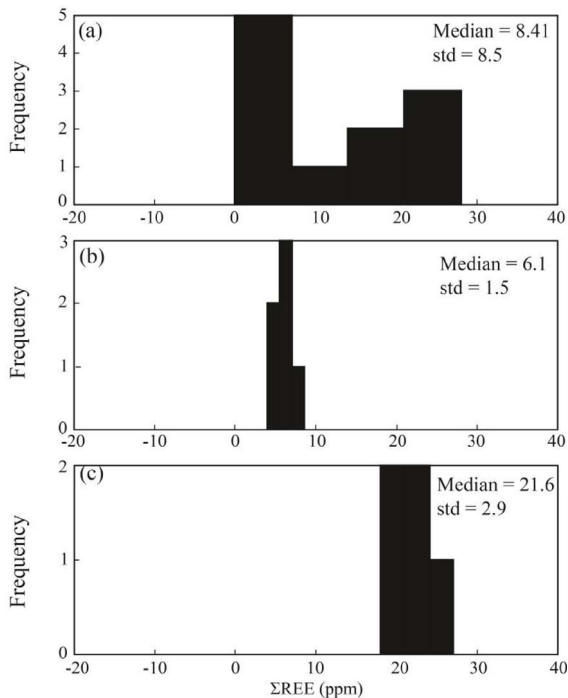
versus fourth tetrad effect values in these samples (Figure 7b, c).

5.3. Mechanism for the occurrence of tetrad effect

Based on the previous researches, the most significant geochemical mechanism for the occurrence of the tetrad effect in various deposits can be categorized as follows [Abedini *et al.*, 2017, Badanina *et al.*,

Table 3. The calculated values for individual tetrad in fluorite samples of the Laal-Kan fluorite deposit

Values	White fluorite		Smoky fluorite		Violet fluorite						
	WF.1	WF.2	SE.1	SE.2	VF.1	VF.2	VF.3	VF.4	VF.5	VF.6	VF.7
T ₁	0.08	0.29	0.05	0.03	0.06	0.26	0.72	0.50	0.47	0.22	0.13
T ₃	0.28	0.06	0.37	0.40	0.25	0.12	0.11	0.08	0.09	0.17	0.43
T ₄	0.16	0.44	0.15	0.31	0.19	0.40	0.30	0.40	0.14	0.35	0.31

**Figure 5.** The frequency diagrams for Σ REE (ppm) in fluorite samples in the Laal-Kan district. (a) Σ REE, (b) first population of Σ REE (FI-1) and (c) second population (FI-2) of Σ REE.

2010, Cao *et al.*, 2013, Irber, 1999, Kawabe, 1995, Monecke *et al.*, 2007, Nardi *et al.*, 2012, Pan, 1997, Rezaei Azizi *et al.*, 2017]: (1) mineral phase fraction during emplacement of an igneous system, (2) the presence of F-complex in fluid/solution, (3) interaction of fluid and melt in the hydrothermal system and (4) alteration processes including hydrothermal and/or weathering.

The fractionation of mineral phases in igneous systems and interaction of the hydrothermal fluids with host rocks during uprising can generate a remarkable convex (M-type) tetrad effect phenome-

non in the separated mineral phases of system [Lee *et al.*, 2013, McLennan, 1994, Wu *et al.*, 2011]. As shown in Figure 6, the chondrite-normalized REE patterns in this deposit have a pronounced convex (M-type) tetrad effect, especially in the third and fourth tetrads. Petrographic and mineralogy studies indicate that the lack of mineral phases such as garnet, monazite and apatite in the fluorite samples of the study district cannot be likely responsible for the occurrence of convex tetrad effect [McLennan, 1994, Pan, 1997].

Figure 8 illustrates the correlation between T₁ tetrad effect values in fluorite samples and some geochemical ratios. As shown in Figure 8a, the early stage fluorite samples are characterized by relatively low T₁ tetrad effect values and high La/Ho ratios, whereas T₁ tetrad effect values display a high/wide range and very low La/Ho ratios that can be due to fractionation of LREE during hydrothermal fluids migration [Bau and Dulski, 1995, Coşanay *et al.*, 2017]. Meanwhile, the bivariate diagram of T₁ tetrad effect values versus Zr/Hf ratios in the studied samples (Figure 8b) indicate that early stage fluorite samples have relatively positive correlation, but the late stage ones have negative correlation. This means that relatively low pH hydrothermal fluids were likely played important role during precipitation of early stage ones and high pH hydrothermal fluids were probably responsible for precipitation of the late stage ones due to interaction of acidic fluids with carbonate host rocks during the migration of fluids [Rezaei Azizi *et al.*, 2018b].

The Y/Ho ratios in the studied samples display wide ranges from chondritic to superchondritic (Figure 8c). The higher Y/Ho ratios in fluorite mineral is an indicative of the role of the existence of ligands such as F⁻, HCO₃⁻, PO₄³⁻, Cl⁻, OH⁻, and CO₃²⁻ in hydrothermal fluids [Migdisov *et al.*, 2016]. During fluorite mineralization, F-rich hydrothermal fluids

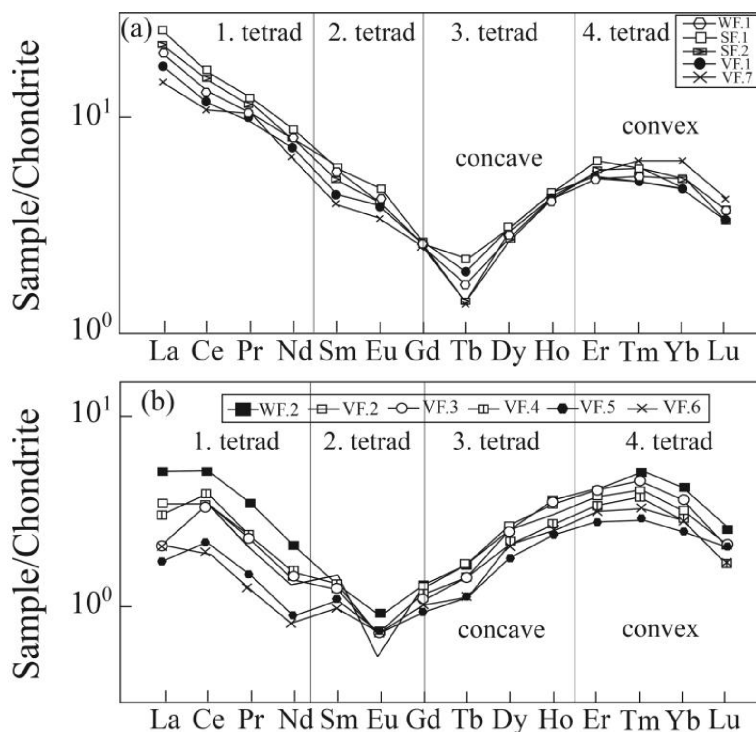


Figure 6. The chondrite-normalized REE patterns for fluorite samples indicating the tetrad fields in the Laal-Kan fluorite deposit. (a) the early stage fluorite samples and (b) the late stage fluorite samples. Normalization values are from Anders and Grevesse [1989].

cause the higher Y/Ho ratio fluorite, but carbonate-rich fluids cause low Y/Ho ratio fluorite to be precipitated [Bühn *et al.*, 2003]. The fluid inclusions studies in this district revealed that the composition of hydrothermal fluids were relatively constant during both the early and late stage fluorite [Rezaei Azizi *et al.*, 2018b]. This means that REE-complex in the presence of F and carbonate ligands were likely responsible for the occurrence of tetrad effect in the fluorite precipitation. Figure 9 shows the T_3 versus T_4 tetrad effect values for fluorite samples in the Laal-Kan deposits. As shown in this figure the early and late stage fluorite samples are also seen in two different and separate fields. The early stage fluorite samples are characterized by high T_3 values but, the late stage ones with low T_3 values. These parameters indicate that the REE distributions in fluorite were probably controlled by tetrad effect phenomenon in this district. Therefore, it can be deduced that the tetrad effect values in fluorite mineralization can be used as a good and powerful geochemical indicator to inter-

pret the physico-chemical conditions and geochemical processes in these types of deposits.

6. Conclusions

Based on the petrographic studies, chemical analysis, the calculated values of first, third and fourth tetrad, REE behavior, Y/Ho, Zr/Hf and La/Ho ratios in the fluorites of the Laal-Kan fluorite deposit, the conclusions can be summarized as follows:

(1) The petrographic studies indicate that fluorite mineralization have been likely occurred in two different stages including early stage fluorite and late stage ones, which are characterized by coarse-grained/massive and fine-grained crystals, respectively.

(2) The chondrite-normalized REE distribution curves of the fluorite samples display a remarkable convex (M-type) tetrad effect curvatures, which is an indicative of hydrothermal/igneous origin in fluids responsible for fluorite precipitations.

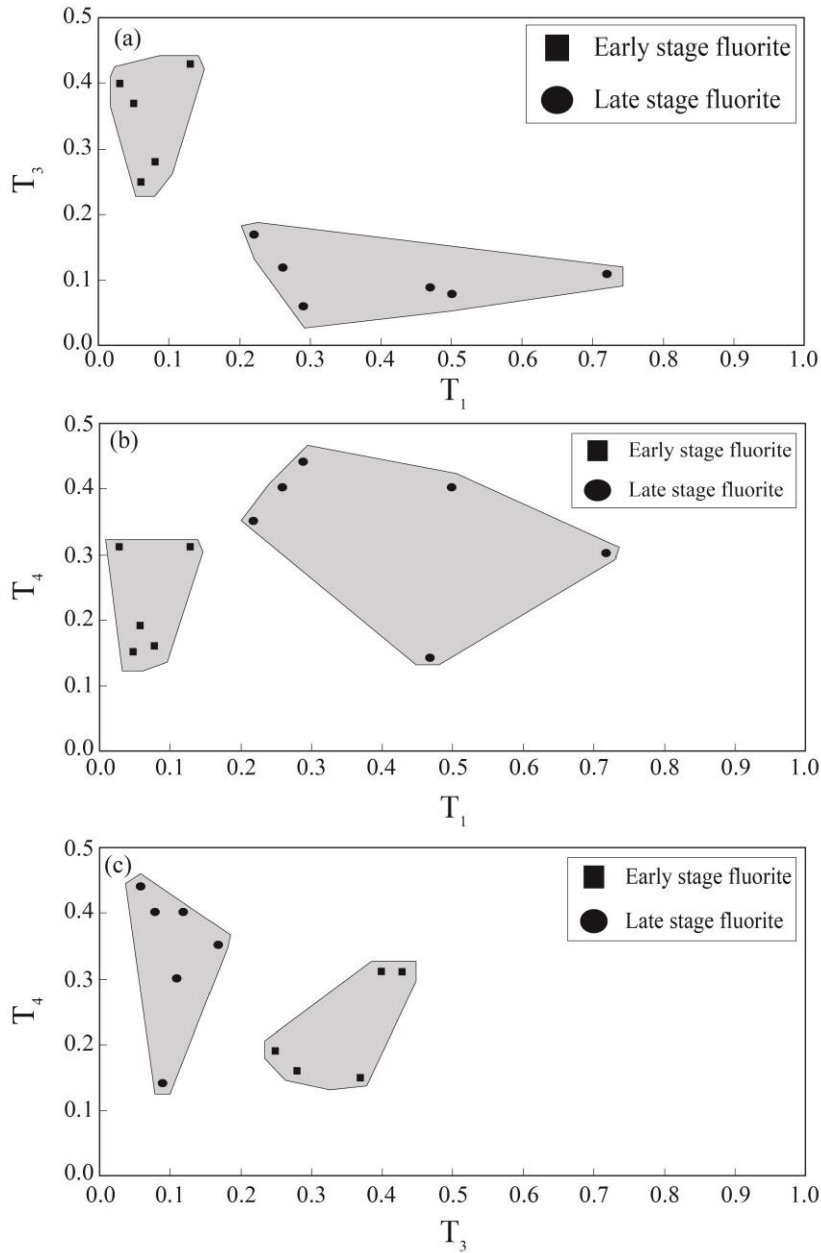


Figure 7. The bivariate diagrams for the calculated tetrad effect values in fluorite samples of the Laal-Kan fluorite deposit. (a) T_1 versus T_3 , (b) T_1 versus T_4 and (c) T_3 versus T_4 .

(3) Based on the relationship between tetrad effect values and some geochemical ratios such as La/Ho, Y/Ho and Zr/Hf it can be concluded that interaction between hydrothermal fluids and carbonate host rocks and REE-F complex were likely the main mechanisms for the occurrence of tetrad effect phenomenon in the study district.

(4) The correlations between T_1 , T_3 and T_4 tetrad effect values of the fluorite samples with geochemical parameters and previous data of fluid inclusions support the idea that fluorite mineralization in this deposit were probably formed from a fluids with relatively constant composition in different stages.

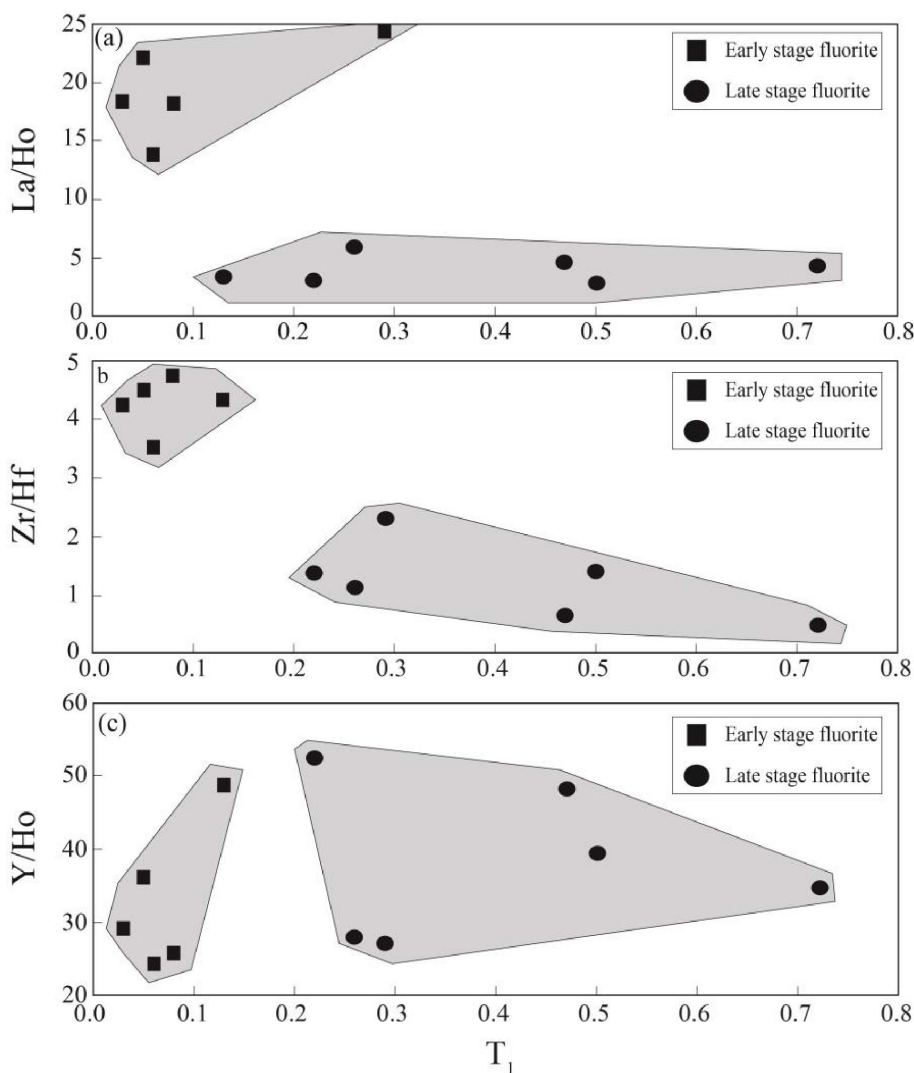


Figure 8. The bivariate diagrams of T_1 tetrad effect values for fluorite samples versus (a) La/Ho, (b) Zr/Hf and Y/Ho ratios in the Laal-Kan fluorite deposit.

(5) The separation of early and late stage fluorite samples in the bivariate diagrams such as T_1 , T_3 and T_4 versus La/Ho, Y/Ho and Zr/Hf can be used a good and powerful geochemical indicator to investigate and interpret the geochemical processes during deposition of fluorite.

Acknowledgements

This work was financially fully supported by the Bureau of Deputy of Research and Complementary Ed-

ucation of Urmia University. We would like to state our thanks and appreciation to the authorities of this bureau. Our gratitude is further expressed to Professor Vincent Courtillot, Dr. Marguerite Godard, and two other anonymous reviewers for reviewing our manuscript and making critical comments and valuable suggestions which have definitely improved the quality of this work.

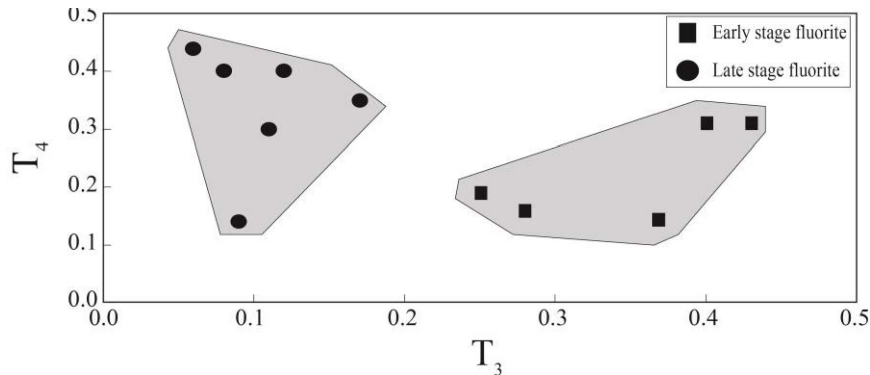


Figure 9. The bivariate diagram of T_3 versus T_4 tetrad effect values for fluorite samples in the Laal-Kan district.

References

- Abedini, A., Calagari, A. A., and Akbari, M. (2011). Geochemistry and genesis of Mehredjan bentonite deposit, southeast of Khor, Isfahan province. *J. Geopersia.*, 1:47–58.
- Abedini, A., Calagari, A. A., and Rezaei Azizi, M. (2018a). The tetrad-effect in rare earth elements distribution patterns of titanium-rich bauxites: evidence from the Kanigorgeh deposit, NW Iran. *J. Geochem. Explor.*, 186:129–142.
- Abedini, A. and Rezaei Azizi, M. (2019). The Hizeh-Jan kaolin deposit of NW Iran: the tetrad effect in REE distribution patterns. *Acta Geol. Sin. Engl.*, 93:74–87.
- Abedini, A., Rezaei Azizi, M., and Calagari, A. A. (2018b). Lanthanide tetrad effect in limestone: a tool to environment analysis of the Ruteh Formation, NW Iran. *Acta Geodyn. Geomater.*, 15:229–246.
- Abedini, A., Rezaei Azizi, M., and Calagari, A. A. (2018c). The lanthanide tetrad effect in argillic alteration: an example from the Jizvan district, northern Iran. *Acta Geol. Sin. Engl.*, 92:1468–1485.
- Abedini, A., Rezaei Azizi, M., and Calagari, A. A. (2019a). REE tetrad effect as a powerful indicator of formation conditions of karst bauxites: a case study of the Shahindezh deposit, NW Iran. *Acta Geol. Sin. Engl.*, 93:912–927.
- Abedini, A., Rezaei Azizi, M., and Calagari, A. A. (2019b). REE Mobility and tetrad effects in bauxites: an example from the Kanisheeteh deposit, NW Iran. *Acta Geodyn. Geomater.*, 15:229–246.
- Abedini, A., Rezaei Azizi, M., Calagari, A. A., and Cheshmehsari, M. (2017). Rare earth element geochemistry and tetrad effects of the Dalir phosphatic shales, northern Iran. *N. Jb. Geol. Paläont. Abh.*, 286:169–188.
- Ackerman, L. (2005). Magmatic vs. hydrothermal origin of fluorites from Vlastejovice Bohemian massif. *J. Czech Geol. Soc.*, 50:35–41.
- Aghanabati, A. (1998). Major sedimentary and structural units of Iran (map). *J. Geosci.*, 7:29–30.
- Akgul, B. (2015). Geochemical associations between fluorite mineralization and A-type shoshonitic magmatism in the Kebane Elazig area, East Anatolia, Turkey. *J. Afr. Earth Sci.*, 111:222–230.
- Alavi, M. (1991). Sedimentary and structural characteristics of the Paleo-Tethys remnants in north-eastern Iran. *Geol. Soc. Am. Bull.*, 103:983–992.
- Alipour, S., Abedini, A., and Talaie, B. (2015). Geochemical characteristics of the Qahr-Abad fluorite deposit, southeast of Saqqez, western Iran. *Arab. J. Geosci.*, 8:7309–7320.
- Anders, E. and Grevesse, N. (1989). Abundances of the elements: meteoritic and solar. *Geochim. Cosmochim. Acta*, 53:187–214.
- Babakhani, A. R. and Ghalamghash, J. (1990). *Geological Map of Iran, 1:100,000 Series Sheet Takht-e-Soleiman*. Geological Survey of Iran, Tehran.
- Badanina, E. V., Syritso, L. F., Volkova, E. V., Thomas, R., and Trumbull, R. B. (2010). Composition of Li-F granite melt and its evolution during the formation of the ore-bearing Orlovka massif in Eastern Transbaikalia. *Petrology*, 18:131–157.
- Badel, M., Angorani, S., and Shariat Panahi, M. (2011). The application of median indicator kriging and neural network in modeling mixed pop-

- ulation in an iron ore deposit. *Comput. Geosci.*, 37:530–540.
- Bau, M. (1996). Controls on the fractionation of isovalent trace elements in magmatic and aqueous systems: evidence from Y/Ho, Zr/Hf, and lanthanide tetrad effect. *Contrib. Mineral. Petrol.*, 123:323–333.
- Bau, M. and Dulski, P. (1995). Comparative study of yttrium and rare earth element behaviours in fluorine-rich hydrothermal fluids. *Contrib. Mineral. Petrol.*, 119:213–223.
- Bau, M., Romer, R. L., Lüders, V., and Dulski, P. (2003). Tracing element sources of hydrothermal mineral deposits: REE and Y distribution and Sr-Nd-Pb isotopes in fluorite from MVT deposits in the Pennine Orefield, England. *Miner. Depos.*, 38:992–1008.
- Bühn, B., Scsneider, J., Dulski, P., and Rankin, A. H. (2003). Fluid-rock interaction during progressive migration of carbonatitic fluids, derived from small-scale trace element and Sr, Pb isotope distribution in hydrothermal fluorite. *Geochim. Cosmochim. Acta*, 67:4577–4595.
- Cao, M. J., Zhou, Q. F., Qin, K. Z., Tang, D. M., and Evans, N. J. (2013). The tetrad effect and geochemistry of apatite from the Altay Koktokay No. 3 pegmatite, Xinjiang, China: implications for pegmatite petrogenesis. *Mineral. Petrol.*, 107:985–1005.
- Castorina, F., Masi, U., Padalino, G., and Palomba, M. (2008). Trace-element and Sr-Nd isotopic evidence for the origin of the Sardinian fluorite mineralization (Italy). *Appl. Geochem.*, 23:2906–2921.
- Coşanay, P., Kirat, E., Çevik, N., Kızılkant, C., Mutlu, H., and Koç, S. (2017). Geochemical, microthermometric, and isotopic constraints on the origin of fluorite deposits in central Anatolia, Turkey. *Turk. J. Earth Sci.*, 26:206–226.
- Deng, X. H., Chen, Y. J., Yao, J. M., Bagas, L., and Tang, H. S. (2014). Fluorite REE-Y (REY) geochemistry of the ca. 850 Ma Tumen molybdenite-fluorite deposit, eastern Qinling, China: constraints on ore genesis. *Ore Geol. Rev.*, 63:532–543.
- Dill, H. G., Luna, L. I., Nolte, N., and Hansen, B. T. (2016). Chemical, isotopic and mineralogical characteristics of volcanogenic epithermal fluorite deposits on the Permo-Mesozoic foreland of the Andean volcanic arc in Patagonia (Argentina). *Chem. Erde.*, 76/2:275–297.
- Edjabou, M. E., Martín-Fernández, J. A., Scheutz, C., and Astrup, T. F. (2017). Statistical analysis of solid waste composition data: arithmetic mean, standard deviation and correlation coefficients. *Waste Manag.*, 69:13–23.
- Ehya, F. (2012). Variation of mineralizing fluids and fractionation of REE during the emplacement of the vein-type fluorite deposit at Bozijan, markazi province, Iran. *J. Geochem. Explor.*, 112:93–106.
- Feng, J. L., Zhao, Z. H., Chen, F., and Hu, H. P. (2014). Rare earth elements in sinters from the geothermal waters (hot springs) on the Tibetan Plateau, China. *J. Volcanol. Geotherm. Res.*, 287:1–11.
- Fidelis, I. and Siekierski, S. (1966). The regularities in stability constants of some rare earth complexes. *J. Inorg. Nucl. Chem.*, 28:185–188.
- Gilg, H. A., Boni, M., and Balassone, G. (2006). Marble-hosted sulfide ores in the Angouran Zn-(Pb-Ag) deposit, NW Iran: interaction of sedimentary brines with a metamorphic core complex. *Miner. Depos.*, 41:1–16.
- Irber, W. (1999). The lanthanide tetrad effect and its correlation with K/Rb, Eu/Eu*, Sr/Eu, Y/Ho, and Zr/Hf of evolving peraluminous granite suites. *Geochim. Cosmochim. Acta*, 63:489–508.
- Jahn, B. M., Wu, F., Capdevila, R., Martineau, F., Zhao, Z., and Wang, Y. (2001). Highly evolved juvenile granites with tetrad REE patterns: the Woduhe and Baerzhe granites from the Great Xing'an Mountains in NE China. *Lithos*, 59:171–198.
- Jorgensen, C. K. (1970). The “tetrad effect” of Peppard is a variation of the nephelauxetic ratio in the third decimal. *J. Inorg. Nucl. Chem.*, 32:3127–3128.
- Kawabe, I. (1995). Tetrad effects and fine structures of REE abundance patterns of granitic and rhyolitic rocks: ICP-AES determinations of REE and Y in eight GSJ reference rocks. *Geochem. J.*, 29:213–230.
- Kawabe, I., Ohta, A., Ishii, S., tokumura, M., and Miyauchi, K. (1999). REE partitioning between Fe-Mn oxyhydroxide precipitates and weakly acid NaCl solutions: convex tetrad effect and fractionation of Y and Sc from heavy lanthanides. *Geochem. J.*, 33:167–180.
- Khosravi, M., Abedini, A., Alipour, S., and Mongelli, G. (2017). The Darzi-Vali bauxite deposit, West-Azarbaidjan Province, Iran: critical metals distribution and parental affinities. *J. Afr. Earth. Sci.*, 129:960–997.
- Lee, S. G., Asahara, Y., Tanaka, T., Lee, S. R., and Lee, T. (2013). Geochemical significance of the Rb-

- Sr, La–Ce and Sm–Nd isotope systems in A-type rocks with REE tetrad patterns and negative Eu and Ce anomalies: the Cretaceous Muamsa and Weolaksan granites, South Korea. *Chem. Erde*, 73:75–88.
- Levresse, G., Tritlla, J., Solorio-Mungua, J. G., Valencia, V., and Linares, P. J. P. (2011). Fluid inclusions and U/Pb dating of the El Pilote Fluorite skarn occurrence: metallogenic implications. *C. R. Geosci.*, 343:342–350.
- Masuda, A., Kawakami, O., Dohmoto, Y., and Takenaka, T. (1987). Lanthanide tetrad effects in nature: two mutually opposite types W and M. *Geochem. J.*, 21:119–124.
- Masuda, A., Matsuda, N., Minami, M., and Yamamoto, H. (1994). Approximate estimation of the degree of lanthanide tetrad effect from precise but partially void data measured by isotope dilution and an electron configuration model to explain the tetrad phenomenon. *Proc. Jpn. Acad. B*, 70:169–174.
- McLennan, S. M. (1994). Rare earth element geochemistry and the “tetrad” effect. *Geochim. Cosmochim. Acta*, 58:2025–2033.
- Migdisov, A., Williams-Jones, A. E., Brugger, J., and Caporuscio, F. A. (2016). Hydrothermal transport, deposition, and fractionation of the REE: experimental data and thermodynamic calculations. *Chem. Geol.*, 439:13–42.
- Minamim, M., Masuda, A., Takahashi, K., Adachi, M., and Shimizu, H. (1998). Y–Ho fractionation and lanthanide tetrad effect observed in cherts. *Geochem. J.*, 32:405–419.
- Monecke, T., Dulski, P., and Kempe, U. (2007). Origin of convex tetrads in rare earth element patterns of hydrothermally altered siliceous igneous rocks from the Zinnwald Sn–W deposit, Germany. *Geochim. Cosmochim. Acta*, 71:335–353.
- Monecke, T., Kempe, U., Monecke, J., Sala, M., and Wolf, D. (2002). Tetrad effect in rare earth element distribution patterns: a method of quantification with application to rock and mineral samples from granite-related rare metal deposits. *Geochim. Cosmochim. Acta*, 66:1185–1196.
- Nardi, L. V. S., Formoso, M. L. L., Jarvis, K., Oliveira, L., Bastos Neto, A. C., and Fontana, E. (2012). REE, Y, Nb, U, and Th contents and tetrad effect in zircon from a magmatic-hydrothermal F-rich system of Sn-rare metalecrolite mineralized granites from the Pitinga Mine, Amazonia, Brazil. *J. South Am. Earth Sci.*, 33:34–42.
- Nkoumbou, C., Gentry, F. C., Numbem, J. T., Lobe, Y. V. B. E., and Keyamfe, C. S. N. (2017). Petrology and geochemistry of REE-rich Mafe’ banded iron formations (Bafia group, Cameroon). *C. R. Geosci.*, 349:165–174.
- Nugent, L. J. (1970). Theory of the tetrad effect in the lanthanide (III) and actinide (III) series. *J. Inorg. Nucl. Chem.*, 32:3485–3491.
- Pan, Y. M. (1997). Controls on the fractionation of isovalent trace elements in magmatic and aqueous systems: evidence from Y/Ho, Zr/Hf and lanthanide tetrad effect- a discussion of the article by M. Bau (1996). *Contrib. Mineral. Petrol.*, 128:405–408.
- Rajabi, A., Rastad, E., and Canet, C. (2012). Metallogeny of Cretaceous carbonate-hosted Zn–Pb deposits of Iran: geotectonic setting and data integration for future mineral exploration. *Int. Geol. Rev.*, 54:1649–1672.
- Rezaei Azizi, M., Abedini, A., Alipour, S., and Bagheri, H. (2018a). REE geochemical characteristics and fluid inclusion studies of the Bagher-Abad fluorite deposit, Central Iran. *N. Jb. Miner. Abh.*, 195:247–263.
- Rezaei Azizi, M., Abedini, A., Alipour, S., and Bagheri, H. (2018b). The Laal-Kan fluorite deposit, Zanjan Province, NW Iran: Constraints on REE geochemistry and fluid-inclusions. *Arab. J. Geosci.*, 11(719):1–16.
- Rezaei Azizi, M., Abedini, A., Alipour, S., Niroomand, S., Sasmaz, A., and Talaei, B. (2017). Rare earth element geochemistry and tetrad effects in fluorites: A case study from the Qahr-Abad deposit, Iran. *N. Jb. Geol. Paläont. Abh.*, 383:255–273.
- Richards, J. P., Wilkinson, D., and Ullrich, T. H. (2006). Geology of the Sari Gunay epithermal gold deposit, northwest Iran. *Econ. Geol.*, 101:1455–1496.
- Sasmaz, A., Kryuchenko, N., Zhovinsky, E., Suyarko, V., Konakci, N., and Akgul, B. (2018). Major, trace and rare earth element (REE) geochemistry of different colored fluorites in the Bobrynets region, Ukraine. *Ore Geol. Rev.*, 102:338–350.
- Sasmaz, A., Önal, A., Sagioglu, A., Önal, M., and Akgul, B. (2005). Origin and nature of the mineralizing fluids of thrust zone fluorites in Celikhan (Adiyaman, Eastern Turkey): a geochemical approach. *Geochem. J.*, 39:131–139.

- Sasmaz, A. and Yavuz, F. (2007). REE geochemistry and fluid-inclusion studies of fluorite deposits from the Yaylagözü area (Yıldızeli-Sivas) in Central Turkey. *N. Jb. Miner. Abh.*, 183(2):215–226.
- Schwinn, G. and Markl, G. (2005). REE systematics in hydrothermal fluorite. *Chem. Geol.*, 216:235–248.
- Shannon, R. D. (1976). Revised effective ionic radii and systematic studies of inter atomic distances in halides and chalcogenides. *Acta Crystallogr. B*, 25:925–946.
- Takahashi, Y., Yoshida, H., Sato, N., Hama, K., Yusa, Y., and Shimizu, H. (2002). W- and M-type tetrad effects in REE patterns for water–rock systems in the Tono uranium deposit, central Japan. *Chem. Geol.*, 184:311–335.
- Tassongwa, B., Eba, F., Njoya, D., Tchakounte, J. N., Jeudong, N., Nkoumbou, C., and Njopwouo, D. (2017). Physico-chemistry and geochemistry of Balengou clay deposit (West Cameroon) with inference to an argillic hydrothermal alteration. *C. R. Geosci.*, 349:212–222.
- Veksler, I. V., Dorfman, A. M., Kamenetsky, M., Dulski, P., and Dingwell, D. (2005). Partitioning of lanthanides and Y between immiscible silicate and fluoride melts, fluorite and cryolite and the origin of the lanthanide tetrad effect in igneous systems. *Geochim. Cosmochim. Acta*, 69:2847–2860.
- Whitney, D. L. and Evans, B. W. (2010). Abbreviations for names of rock-forming minerals. *Am. Mineral.*, 95:185–187.
- Williams, M. R., Holwell, D. A., Lilly, R. M., Case, G. N. D., and McDonald, I. (2015). Mineralogical and fluid characteristics of the fluorite-rich Monakoff and E1 Cu-Au deposits, Cloncurry region, Queensland, Australia: implications for regional F-Ba-rich IOCG mineralization. *Ore Geol. Rev.*, 64:103–127.
- Wu, C. Z., Liu, S. H., Gu, L. X., Zhang, Z. Z., and Lei, R. X. (2011). Formation mechanism of the lanthanide tetrad effect for a topaz and amazonite-bearing leucogranite pluton in eastern Xinjiang, NW China. *J. Asian Earth Sci.*, 42:903–916.